Evolution of Thrace Macula on Europa: Strike-slip tectonic control and Identification of the youngest terrains

Pietro Matteoni[1], Alicia Neesemann[1], Ralf Jaumann[1], Jon Hillier[1] and Frank Postberg[1]

[1] Planetary Sciences and Remote Sensing, Institute of Geological Sciences, Freie Universität Berlin, Germany

Corresponding author: Pietro Matteoni (pietro.matteoni@fu-berlin.de)

Key Points:

- We conducted a structural analysis on Thrace Macula, a chaotic terrain on Europa, using imaging and newly processed topographic data
- We found that preexisting strike-slip faults border Thrace Macula and have constrained its emplacement and areal distribution
- We provide insights into the history of Thrace and identify it as a prime location for future missions to sample fresh subsurface material

Abstract:

Chaos terrains are geologically young and extensively disrupted surface features of Europa, thought to be an expression of the subsurface ocean interacting with the surface. The most prominent examples of this terrain on Europa are Conamara Chaos, and Thera and Thrace Maculae, all prime targets for the upcoming JUICE and Europa Clipper missions to assess the astrobiological potential of Europa. Of the three features, Thrace Macula is currently the least studied and understood. It intersects both Agenor Linea to the north and Libya Linea to the south, two important regional-scale bands whose interaction with Thrace is yet to be fully unraveled, especially in terms of their relative ages of emplacement and activity. Through detailed structural mapping using Galileo Solid State Imager data and terrain analysis on Digital Terrain Models, we here develop a novel hypothesis on the mechanisms that have been involved in the study area. We find that Thrace Macula is bordered along most sides by preexisting strike-slip faults that have constrained its emplacement and areal distribution. We determine a sequence of events in the area involving the formation of Agenor Linea, followed by that of Libya Linea first and Thrace Macula later, and ultimately by strike-slip tectonic activity driven by Libya Linea and displacing a portion of Thrace Macula. Therefore, Thrace's subsurface material, uprising along faults postdating its formation, likely represents the freshest possible that could be sampled by future spacecraft in this region, a major consideration for the upcoming Europa Clipper mission.

Plain Language Summary:

Europa, an icy moon of Jupiter, has unique surface features known as chaos terrains, believed to result from interactions between its subsurface ocean and surface. Of these terrains, Conamara Chaos and Thera and Thrace Maculae are prime targets for upcoming missions to investigate the astrobiological potential of Europa. However, Thrace Macula, which is situated between Agenor Linea to the north and Libya Linea to the south (two large-scale bands, linear geological features), remains poorly understood. In this study, we used detailed mapping of faults and lineaments, together with topographical analysis, to propose a new hypothesis for the formation and evolution of Thrace Macula. Our findings suggest that preexisting tectonic faults constrained its emplacement and distribution, while a sequence of events starting with the formation of Agenor Linea, followed by Libya Linea first and Thrace Macula later, culminated in strike-slip tectonic activity driven by Libya Linea that displaced a portion of Thrace Macula. These results imply that future spacecraft could sample Thrace's subsurface material uplifting along faults postdating its formation, the freshest available in this region. This research sheds light on Europa's regional history and its astrobiological potential.

1 Introduction

Chaos terrains on Europa are geologically very young (Doggett et al., 2009; Figueredo & Greeley, 2004) and extensively disrupted surface features, generally consisting of blocks of preexisting terrain within a hummocky matrix material (Collins & Nimmo, 2009). Chaos is one of the major terrain types found on Europa, covering ~25–40% of the surface (Collins & Nimmo, 2009; Figueredo & Greeley, 2004). While typically considered compositionally distinct from their surroundings due to their reddish-brown color, likely from hydrated sulfates (Dalton et al., 2005) or sulfuric acid hydrate (Carlson et al., 1999), some leading-hemisphere chaos regions have recently been shown to probably have material contributions from endogenous sodium chloride sourced from a subsurface ocean (Trumbo et al., 2019a, 2019b, 2022). Chaos disrupts the preexisting ridged and banded terrain to varying degrees. In some chaos regions, large blocks are left relatively intact and the ridged terrain preserved on the block tops can be used to infer the relative degree of translation, rotation, and tilting experienced by the blocks (Spaun et al., 1999). The formation of Europa's chaos has been intensely debated, with hypotheses including melt-through (e.g., Greenberg et al., 1999; O'Brien, 2002), diapirism (e.g., Pappalardo et al., 1998; Schenk & Pappalardo, 2004), and the collapse of a melt-lens within the ice shell (e.g., B. E. Schmidt et al., 2011; Soderlund et al., 2014). Collins & Nimmo (2009) propose a set of both hard and soft constraints for each chaos formation hypothesis, based on observations of chaos terrains. They note that any chaos formation mechanism must appropriately account for several observational constraints: the matrix and block characteristics, including high and low topographies, block translation and rotation, exposure of hydrated salts and/or acids, large range in planform size (1–1,000 km in diameter), and broad global distribution. Similarly, models should consider the relationship between chaos and Europa's pits and domes (or lenticulae), preservation and destruction of preexisting terrains, and chaos growth through coalescence. Leonard et al. (2018) suggest that each of the currently proposed mechanisms for chaos formation can account for only a portion of these constraints, hinting at the fact that chaos terrains could potentially be formed by a combination of such mechanisms. The ongoing

uncertainty surrounding the formation of Europa's chaos terrains, and their relatively young surface age (Doggett et al., 2009; Figueredo & Greeley, 2004; Prockter & Schenk, 2005; B. E. Schmidt et al., 2011), make these regions of particular interest for studies of Europa's habitability. Previous studies hypothesize that chaos terrains are an expression of the subsurface ocean interacting with the surface, whether the exchange is occurring through the solid, frozen transport of icy materials (e.g., Howell & Pappalardo, 2018; Johnson et al., 2017; Kattenhorn & Prockter, 2014), or via the formation, migration, and eruption of liquid water and brines (e.g., Greenberg et al., 1999; B. E. Schmidt et al., 2011), or viscous lavas (Quick et al., 2017). The exchange of material between the surface and subsurface of Europa may be critical to sustaining the chemical disequilibria that could support the emergence or persistence of habitable environments and, potentially, life (Hand et al., 2007, 2009; Vance et al., 2016). Thus, determining how chaos terrains form is an important key to assessing the habitability potential of Europa's icy shell and subsurface ocean.

The largest and most well-studied example of chaos terrain on Europa is Conamara Chaos (e.g., Carr et al., 1998; Greenberg et al., 1999; Head & Pappalardo, 1999; Schenk & Pappalardo, 2004), characterized by a quasi-circular shape and seemingly floating ice blocks (up to several km in size), standing out topographically from its lower surroundings and seeming to contain raised lower-albedo matrix 'domes' (B. E. Schmidt et al., 2011; Spaun et al., 1999). Another prominent example of Europan chaos terrain is Thrace Macula (Figure 1), slightly smaller - both in terms of areal distribution and coverage in the literature- yet still one of the largest chaos regions on Europa, visible in global-scale images because of its large extent and low relative albedo (Figure 1). Centered at 46°S; 172°W in the southern trailing hemisphere of Europa, Thrace intersects the prominent linear bands Agenor Linea to the northwest, and Libya Linea to the south. It extends for ~220 km in the NNE-SSW direction along its major axis and ranges in width between 25 and 60 km. Its distinct lobate margins led to early suggestions that Thrace Macula formed from cryomagmas effusively emplaced on the surface (Miyamoto et al., 2005; Wilson et al., 1997), however, higher resolution Galileo images showed that Thrace is a type of chaos, a region in which the surface appears to have been significantly disrupted. Preliminary mapping of Thrace Macula by Kortz et al. (2000) showed that it did not exhibit the intense breakup, rotation, and translation of plates that have been documented in other chaos regions such as Conamara Chaos (e.g., Spaun et al., 1999). Instead, these authors further noted that the boundary between Thrace and its surroundings is more transitional than at Conamara and characterized by evidence of embayment. Most significantly, they noted that multiple preexisting linear features can be traced into and across the macula, indicating in-situ modification. Kortz et al. suggested brine mobilization as a candidate process that might account for these observations. Thrace Macula has been further interpreted as the result of disruption and darkening of the existing surface by a thermal source (diapir or freezing liquid body) impinging from below, that may have mobilized near-surface brines to produce the dark, low-lying deposits (Fagents, 2003). Only at Thrace's margins is there reliable evidence of low-viscosity fluids confined by the preexisting topography of the background ridged plains (Fagents, 2003). According to topographic data analysis, the interior of Thrace seems to lie at or slightly above the elevation of the surrounding terrain (Prockter & Schenk, 2016; B. E. Schmidt et al., 2012). Another nearby large chaos region, Thera Macula, was shown to have a very different morphology and topography, displaying large blocks of preexisting terrain and being relatively low with respect to the surrounding terrain. This has been explained as the result of subsidence and disaggregation of existing terrain due to the presence in its immediate subsurface of a currently liquid melt lens

(B. E. Schmidt et al., 2011). A similar origin for Thrace Macula has been invoked while considering it as being at a later stage in such an evolutionary model and therefore being older than Thera (B. E. Schmidt et al., 2012). Therefore, the origins of Thrace Macula remain debated and overall less investigated, compared to Thera (Fagents et al., 2022).

Given the relatively young age of these features and potential evidence of emplacement at the surface of material originating from within Europa's interior, both Thera and Thrace maculae are sites of high interest for the upcoming *Europa Clipper* mission with two spacecraft flybys over their locations planned (Lam et al., 2018). Of specific interest will be the compositional measurements by the Surface Dust Analyzer (SUDA, Kempf et al., 2014) instrument. During these low-altitude flybys, SUDA will acquire in situ mass spectra of ice grains knocked off the surface by the ambient micrometeoroid bombardment (e.g., Krivov et al., 2003) and subsequently encountered by the spacecraft. By back-tracing to their point of origin (Goode et al., 2021, 2023), compositional mapping of the chaos terrains will be possible (Postberg et al., 2011). Therefore, considering its geological significance and the lack of previous thorough investigations of Thrace Macula, we selected this feature and its surrounding areas as the focus of the present study in preparation for the *Europa Clipper* mission.

2 Data and Methods

Digital Terrain Models (DTMs) of the selected areas have been produced using the photoclinometry (PC) technique (e.g., Schenk & Pappalardo, 2004), through the Ames Stereo Pipeline (ASP, Beyer et al., 2018) Shape-from-Shading (SfS) tool (Alexandrov & Beyer, 2018). DTMs were derived from *Galileo*'s Solid-State Imager (SSI) images (Belton et al., 1992), which were processed through the Integrated Software for Imagers and Spectrometers (ISIS 4.4.0, https://isis.astrogeology.usgs.gov/7.0.0/index.html). For the processing of *Galileo* SSI raw image data, we used the SPICE smithed kernels and projected the processed data on a spheroid with a radius of 1560.800 km (i.e., the IAU-defined mean radius for Europa), which is therefore also the DTMs' reference height (Bland et al., 2021a). Photogrammetrically controlled image mosaics were used as background (Bland et al., 2021b).

The PC/SfS technique overcomes the lack, on Europa, of having the same surface area covered by two or more images for traditional stereophotogrammetry DTM production. The smoothness parameter μ of the SfS tool, which weighs the smoothness of the resulting DTM and depends on surface properties, plays an important role and can vary the results significantly: optimal μ values with a good signal-to-noise ratio of the resulting DTM need to be found by trial and error, where different values need to be applied for each image (a detailed description of how μ affects the resulting DTMs can be found in Lesage et al., 2021). Manual quality checks have been conducted through features' height (H) estimation based on shadow length (L) and solar elevation angle (α): $H = L\tan(\alpha)$. The SfS tool assumes uniformity in albedo and photometric parameters across the whole image, based on the reflectance model used. Even though such properties can change at regional or local scales, the overall uncertainties on the SfS DTMs vertical resolution are likely not more than 10-15%, as previously discussed in the literature (Bierhaus & Schenk, 2010; Bland et al., 2021b; Lesage et al., 2021; Schenk et al., 2020; Schenk & Pappalardo, 2004). As well as these estimated average errors, we observe another relative error, based on varying surface properties. As mentioned in Section 1, Thrace Macula exhibits a significantly lower albedo in contrast to the surrounding bright surface of Europa. Thus, the requirements (uniform surface properties) for accurate DTM reconstruction by SfS are unfulfilled. In practice, this leads the SfS algorithm to misinterpret the low albedo of Thrace

Macula as shadows, putting it topographically below the surrounding bright surface. We are fully aware of this inadequacy, and thus limited the tracing of topographic profiles to either high albedo units (e.g., the ridged plains surrounding Thrace Macula), or low albedo ones (e.g., those forming Thrace Macula), without tracing "cross-albedo" profiles that could have been misinterpreted. Therefore, the DTM we produced through PC/SfS accurately represents (vertical resolution uncertainties not higher than 10-15%, as discussed above) the topography of either the low or the high albedo parts of the study area. We further conducted structural mapping of the selected areas on SSI images 9765r, 9978r, and 9980r in stereographic projection (image frames resolution of ~44 m/pixel, which corresponds to a nominal map scale of 1:88,000) using QGIS3 (QGIS.org, 2022. QGIS Geographic Information System. QGIS Association http://www.qgis.org) linear structural features such as faults were identified based on distinctive morphologies such as scarps and lateral offsets, paired with topographical analysis of the DTMs. The structural mapping was also conducted on the regional SSI images 4413r and 4414r (~220 m/px resolution) and the global image mosaic (~500 m/px resolution). The scientific color map *batlow* (Crameri, 2021) is used in the DTM presented in this study, to prevent visual distortion of the data and exclusion of readers with color-vision deficiencies (Crameri et al., 2020).

3 Results

Within the study area, we produced high-resolution DTMs of the 9765r, 9978r, and 9980r SSI image frames (Figure 2), using the PC/SfS technique described in Section 2.

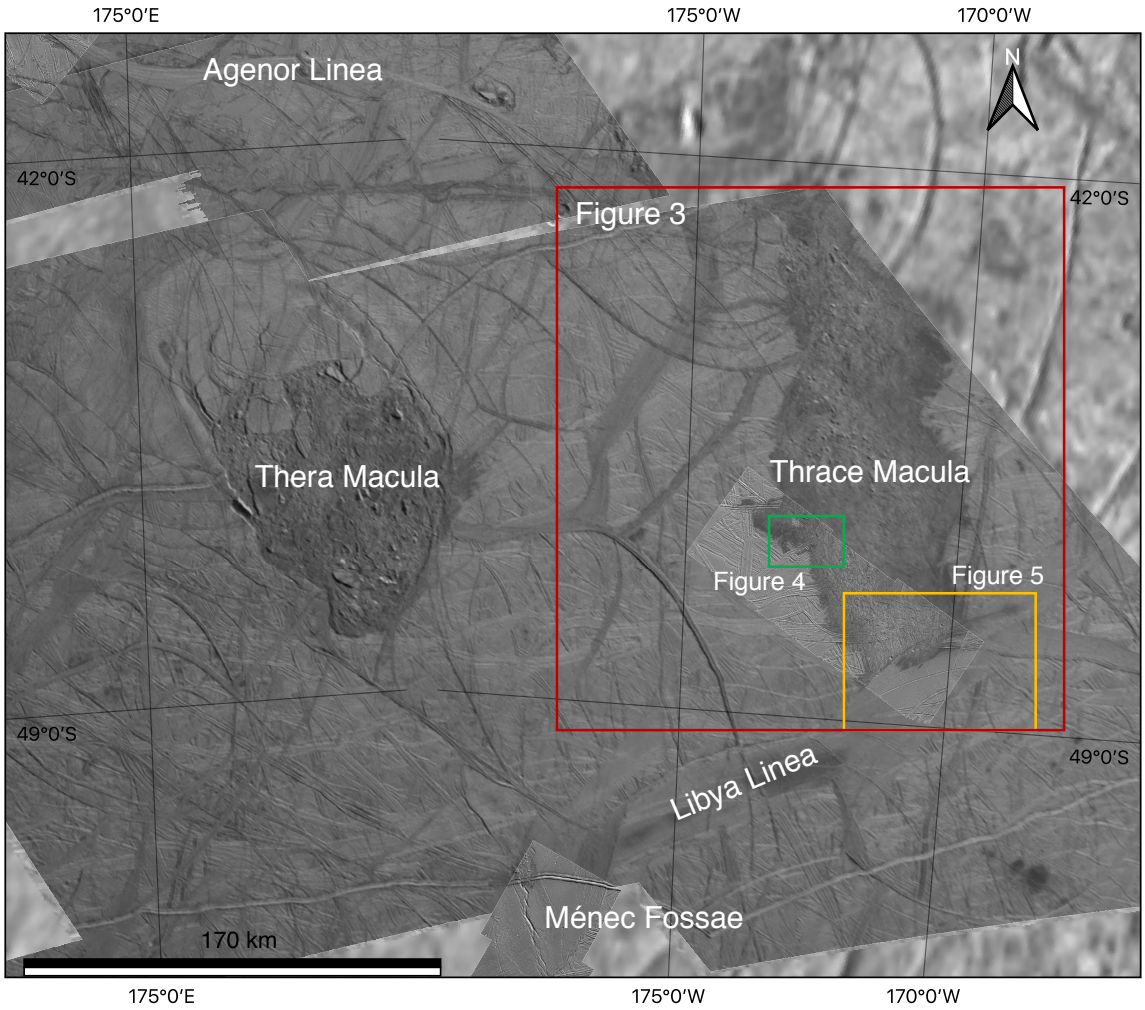

Figure 1. Regional map on photogrammetrically controlled *Galileo* SSI image mosaics, the red box depicts the study area, represented in Figure 3, locations of other figures are also shown. To the SW of the study area, Ménec Fossae is recognizable, while Thera Macula is located to the W. Agenor Linea is a large-scale bright band, located to the NW of Thrace Macula, while Libya Linea, a large-scale smooth band, intersects Thrace Macula at its southern tip along a SW-NE trend. The local *Galileo* SSI images 9765r, 9778r, and 9800r at the southernmost portion of Thrace Macula have ~44 m/px resolution, the surrounding regional SSI images 4413r and 4414r have ~220 m/px resolution, while the background global image mosaic has a resolution ~500 m/px.

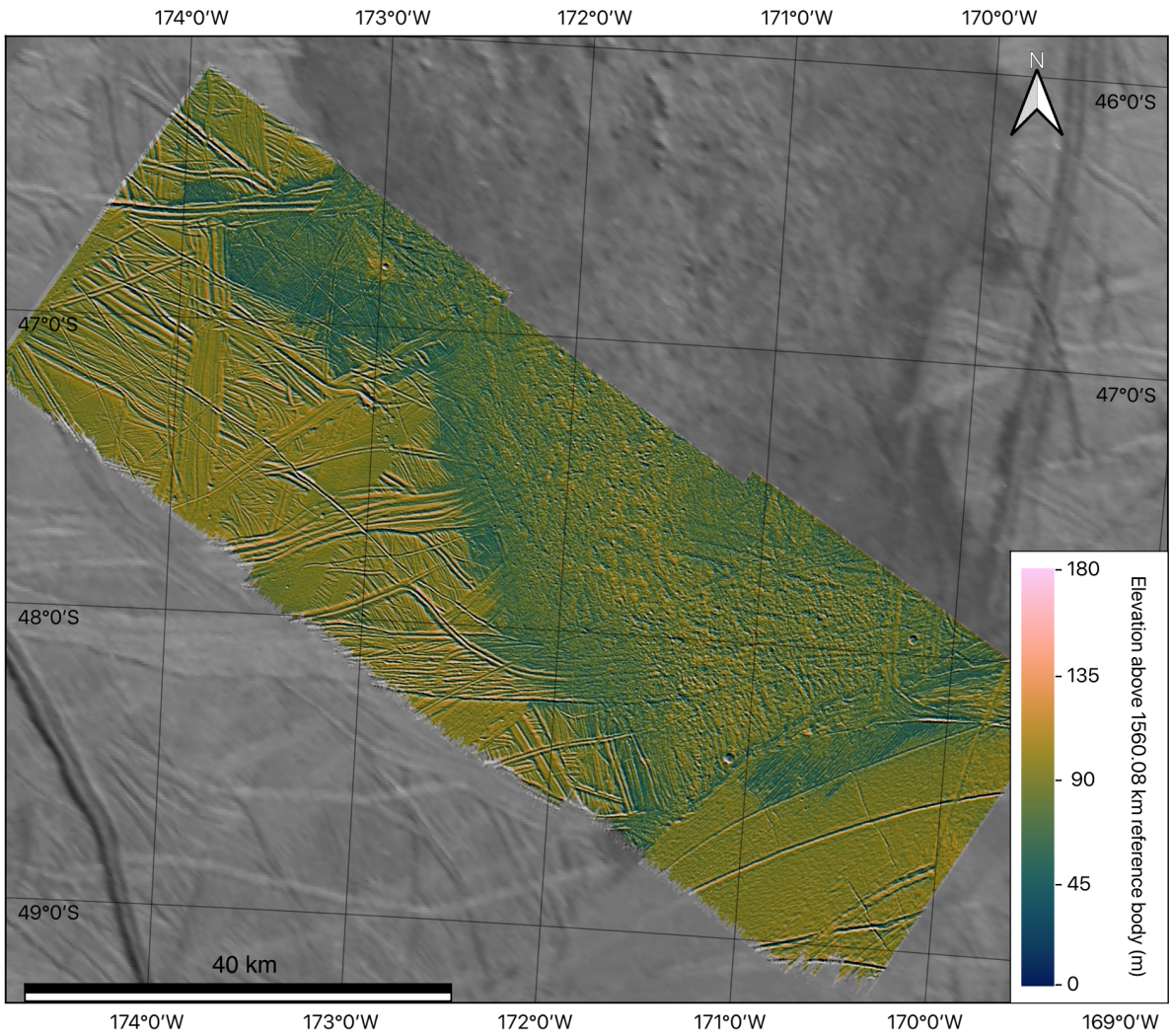

Figure 2. Regional DTM of the southern portion of Thrace Macula, individual DTMs are of 9765r, 9778r, and 9800r *Galileo* SSI image frames, later mosaicked together. The DTM has smoothness parameter (μ) values of 0.001 for each image frame. Image centered at 47.5°S; 172°W.

We identified and mapped several lineaments in the surroundings of Thrace Macula (Figure 3). As some structural and geomorphological mappings of this area had already been conducted (Kortz et al., 2000; Prockter & Schenk, 2016), we focused our study on mapping those lineaments that either (class 1) display clear lateral offsets of preexisting features, i.e., strike-slip faults, or (class 2) those secondary features that can be related to major strike-slip structures. We analyzed both high-resolution *Galileo* SSI images (9765r, 9778r, and 9800r; ~44 m/px) at the southernmost portion of Thrace Macula and the low-resolution 4413r and 4414r (~220 m/px) SSI images. The lower resolution of the latter images limited the accuracy of the analysis, but major lineaments' trends are still identifiable. Our geomorphological interpretation

of different units within the high-resolution images' area is based on the detailed geomorphological map of Prockter & Schenk (2016).

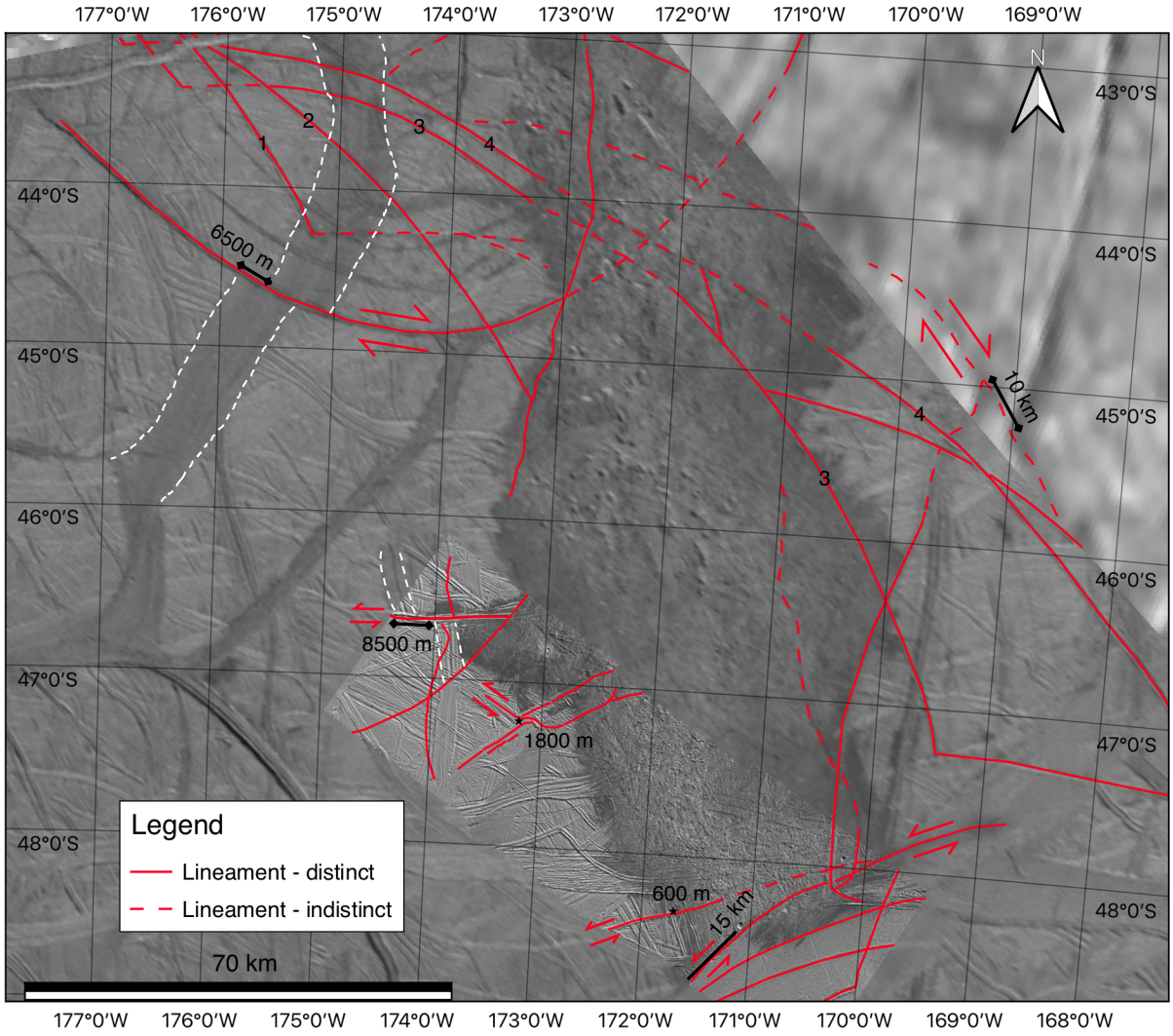

Figure 3. Selected mapping of lineaments, in the area of Thrace Macula, as shown by the red rectangular inset in Figure 1. Thrace Macula is bordered along most sides by linear strike-slip features. Some measured offsets are shown, and arrows indicate the sense of motion where determinable. Various smaller-scale areas are shown in subsequent figures (Figures 4 and 5, locations shown in Figure 1). Numbered features (1-4) represent tailcracks, secondary tension fractures, formed at Agenor Linea's eastern tip, see Section 4.

The structural mapping we conducted is displayed in its entirety in Figure 3, subsequent figures (Figures 4 and 5) contain details of selected areas. We identified ~100 segments of lineaments that fit our classifying criteria of either (class 1) displaying clear lateral offsets of

preexisting features, i.e., strike-slip faults, or (class 2) those secondary features that can be related to major strike-slip structures.

Developing from the NW of the mapped area and originating from the eastern tip of the bright band Agenor Linea, four of these lineaments (numbered 1-4 in Figure 3) fall into the second class, as discussed in detail in Section 4. These extend across the mapped area for several hundred km, in a roughly NW-SE trend, becoming indistinct where they intersect Thrace Macula while being again clearly distinguishable where they are not overlapping with Thrace and seem to terminate at the SE of the mapped area.

In the northern part of the mapped area, several other lineaments intersect Thrace Macula at various locations, also becoming indistinct and altered. Among these, one displays lateral offsets up to 6.5 km (45.5°S; 175.5°W, Figure 3), while another lineament, which displays clear lateral offsets outside of the mapped area to the north, borders Thrace Macula at its north-easternmost extent (very low-resolution imaging, but the contact is still distinguishable, Figure 3 from 43°S; 173°W to 45.8°S; 173.2°W), continues towards the south at the center of Thrace, and ultimately terminates bordering it to the west (45.8°S; 173.2°W). All these features, therefore, fall into the first class of our criteria.

Within the high-resolution images 9765r, 9778r, and 9800r, covering the southern tip of Thrace Macula, we could identify several features that fall into our first class (i.e., those lineaments classified as strike-slip faults). Some of these lineaments have indeed lateral offsets of 1.8 km (47.3°S; 173.2°W, Figures 3 and 4a), 10 km (45.2°S; 169°W, Figure 3), 600 m (48.4°S; 172°W, Figures 3 and 5a), 8.5 km (47.3°S; 174.2°W, Figure 3). One ridged band displaying a 60-70 m deep trough (Figure 4b, topographic information from DTM; geomorphological units from Prockter & Schenk, 2016) crosscuts at a left bend another ridged band, with a measurable left-lateral displacement of 1.8 km (Figure 4a, 47.3°S; 173.2°W). Along the latter feature, some very small-scale transtensional features (probably pull-apart basins - i.e., basins generated in transtensional tectonic settings; e.g., Gürbüz, 2010) are present (around 47.5°S; 173.3°W, Figure 4b), suggesting its likely strike-slip nature, even though lateral offsets are not clearly identifiable along it. Around 48.4°S; 172°W, one ridge-like fault (Kattenhorn, 2004) crosscuts several other features with a constant left-lateral offset of 0.6 km and then continues towards the NNE into Thrace Macula (48.4°S; 172°W, Figure 5a), becoming extremely altered and almost unidentifiable. From relative offset directions, we can infer a left-lateral movement along it.

267

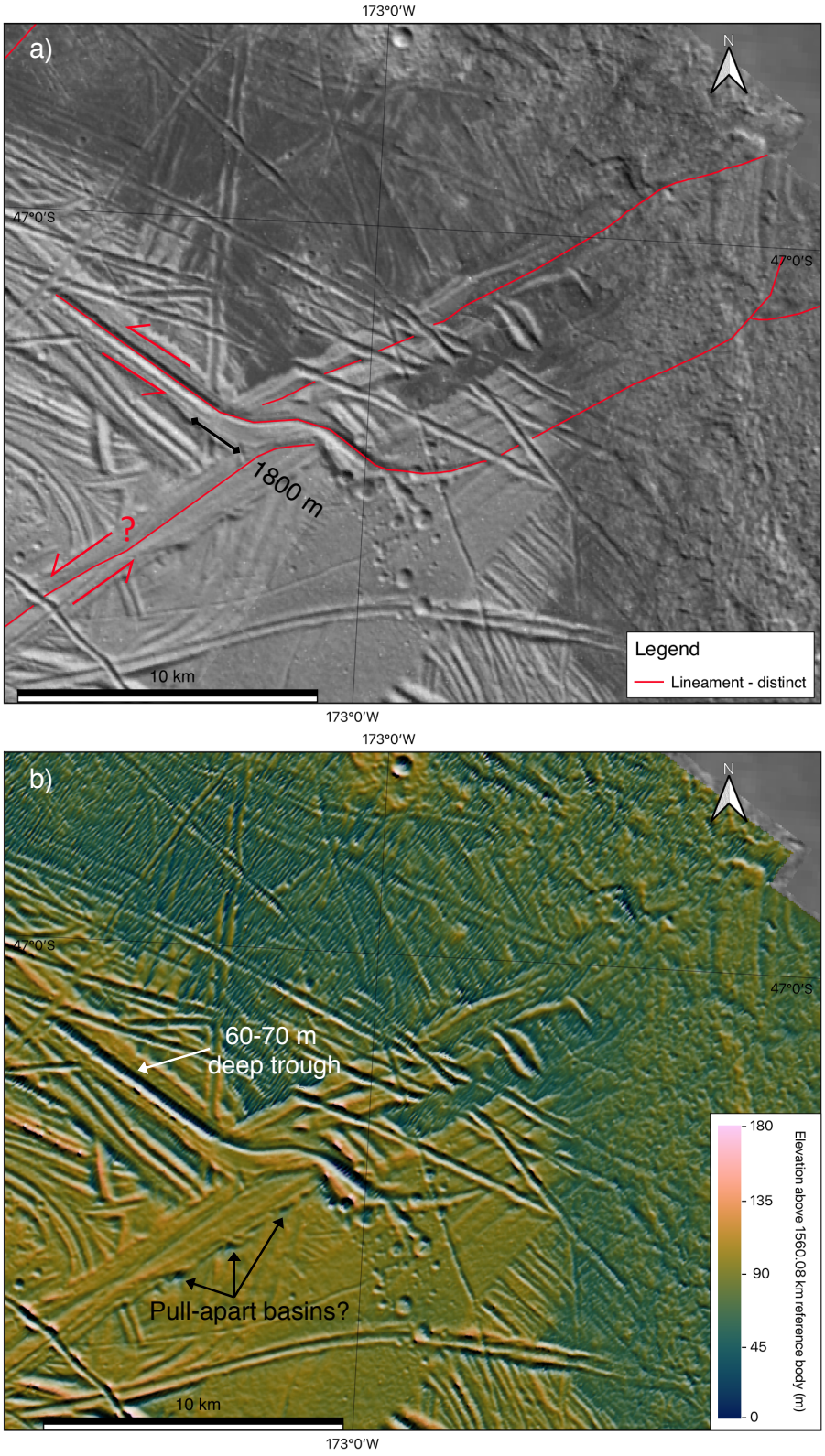
173°0'W
a)
N
47°0'S
47°0'S
1800 m
?
10 km
Legend
Lineament - distinct
173°0'W
173°0'W
b)
N
47°0'S
47°0'S
60-70 m
deep trough
Pull-apart basins?
10 km
180
135
90
45
0
Elevation above 1560.08 km reference body (m)
173°0'W

268

Figure 4. Inset contained within the green rectangle in Figure 1. (a) Interaction of different structural lineaments belonging to distinct tectonic regimes. A lateral offset of ~1800 m is present, generated by a NW-SE oriented sinistral strike-slip ridged band, onto an older NE-SW oriented ridged band. The morphology of the smooth dark material at the center of the figure is an example of embayment and confinement by topographic obstacles, described in Section 3. (b) Topographic data derived from DTM. We infer the presence of at least three small pull-apart basins, related to the NE-SW oriented lineaments. The multiple parallel lines present, particularly in the northern part of the image, represent artifacts of the DTM, which have been reduced to the minimum possible extent but could not be completely removed.

Towards the boundaries of Thrace Macula, smooth dark material embays low-lying areas and is commonly confined by topographic obstacles. This effect is most evident at the NW edge of the high-resolution images (between 46.5°S; 174°W and 47°S; 173°W, Figure 2), at 47.3°S; 172.8°W (Figure 4), and along the contact Thrace-Libya Linea (around 48.4°S; 170.5°W Figure 5a), whose other observed characteristics are hereafter described.

At the southernmost portion of Thrace, several structures depict its complex interaction with the smooth band Libya Linea, against which parts of Thrace truncate abruptly (Figure 5a). The contact between these two very different terrains is sharp and occurs along a curved line, with dark material only present close to the contact in the central and northern parts of the high-resolution image 9800r, while being absent along the southern portion of the contact. The curved lineament marking the contact between Thrace Macula and Libya Linea continues to the NE for several additional km, around which dark material can be seen (white dashed line in Figure 5b).

We interpret this phenomenon as being related to a left-lateral strike-slip fault that represents the contact between Thrace Macula and Libya Linea (indicated as 1 in Figure 5a), with a ~15 km lateral offset (Figure 6). Some additional lineaments (indicated as 2 and 3 in Figure 5a), subparallel to fault 1, are present within Libya Linea. Yet, it is not possible to infer their nature, as no clear lateral displacement is visible and no other tectonic indicators are present. However, the patch of dark material (centered at 48.4°S; 170.5°W, indicated as 4 in Figure 5a) stops abruptly at the contact with lineament 2, except for a very small patch present to the south of lineament 2 (Figure 5a). Within the low-resolution images, along the eastern part of the Thrace Macula-Libya Linea contact, a 26 km extensional displacement with a minor lateral component (i.e., likely a transtensional motion) is clearly identifiable between two portions of a low albedo double ridge (centered at 48.5°S; 169.5°W, yellow dashed line in Figure 5a).

Another lineament (indicated as 5 in Figure 5a) seems to crosscut all the above-mentioned features. Even if its northernmost extent corresponds with the edge of the high-resolution image 9800r, which complicates the interpretation, lineament 5 does not appear to continue further north in the corresponding low-resolution image. This lineament has the morphological characteristics of a ridge and the structures formed at its southern tip are identifiable as tailcracks, curved secondary tension fractures generated at the tip of slipping interfaces and faults. Tailcracks oriented clockwise from the tip indicate dextral shearing, while those oriented counterclockwise from the tip indicate sinistral shearing (Kattenhorn, 2004; Kattenhorn & Marshall, 2006). In the present case, tailcracks are formed at an angle of 70.5° in a clockwise orientation with respect to the strike of the fault and therefore indicate a right-lateral relative movement for their parent feature (Kattenhorn, 2004; Prockter et al., 2000).

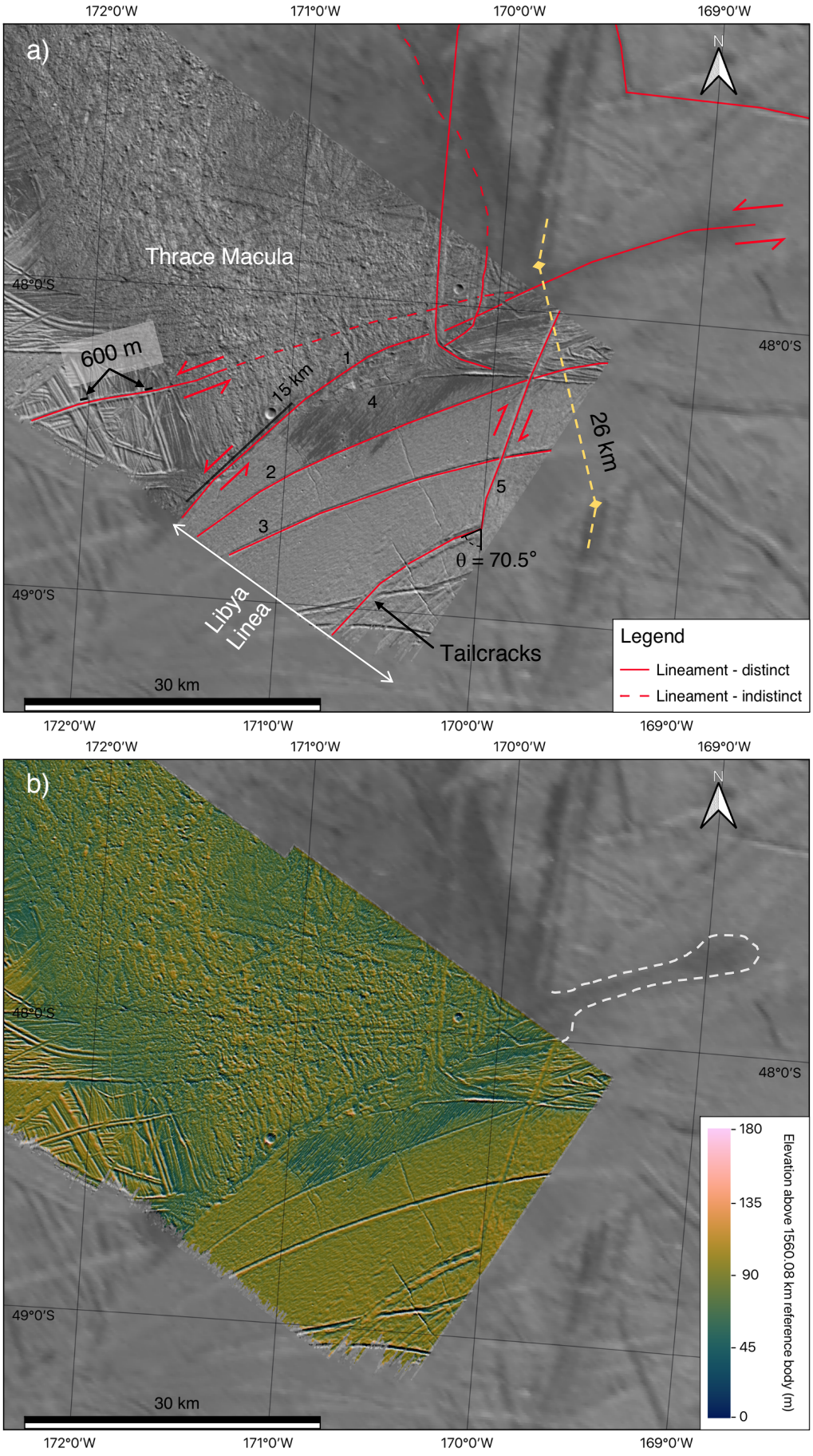
a)
172°0′W
171°0′W
170°0′W
169°0′W
N
Thrace Macula
48°0′S
49°0′S
600 m
15 km
26 km
1
2
3
4
5
θ = 70.5°
Libya Linea
Tailcracks
30 km
Legend
Lineament - distinct
Lineament - indistinct
b)
180
135
90
45
0
Elevation above 1560.08 km reference body (m)

Figure 5. Inset contained within the yellow rectangle in Figure 1, depicting the transitional area between the chaos terrain Thrace Macula and the smooth band Libya Linea. (a) Annotated structural map. The presence of a left-lateral strike-slip fault along the contact between Thrace Macula and Libya Linea (indicated as 1) suggests that such tectonic activity has displaced a portion of Thrace, as dark material (centered at 48.4°S; 170.5°W, indicated as 4) most likely originating from Thrace (along with other features belonging to Thrace present along the contact) is displaced by ~15 km from the SW towards the NE. Some additional lineaments (indicated as 2 and 3) subparallel to fault 1 are present within Libya Linea, yet it is not possible to infer their nature as no clear lateral displacement is visible, nor other tectonic indicators are present. However, the patch of dark material indicated as 4 stops abruptly at the contact with lineament 2, except for a very small patch present to the south of it. The lineament indicated as 5 displays tailcracks formed at an angle of 70.5° in a clockwise orientation with respect to the strike of the fault, which indicate a right-lateral relative movement for their parent feature (see Section 3). A 26 km extensional displacement with a minor lateral component (i.e., likely a transtensional motion) is present between two portions of a low albedo double ridge (centered at 48.5°S; 169.5°W, yellow dashed line). (b) Topographic data derived from DTM. The white dashed line highlights the dark material patch located to the NE of Thrace Macula, along fault 1. The highlighted area likely represents fresh subsurface material originating from Thrace that has infiltrated along fault 1 and has spread on the surface (see Section 4).

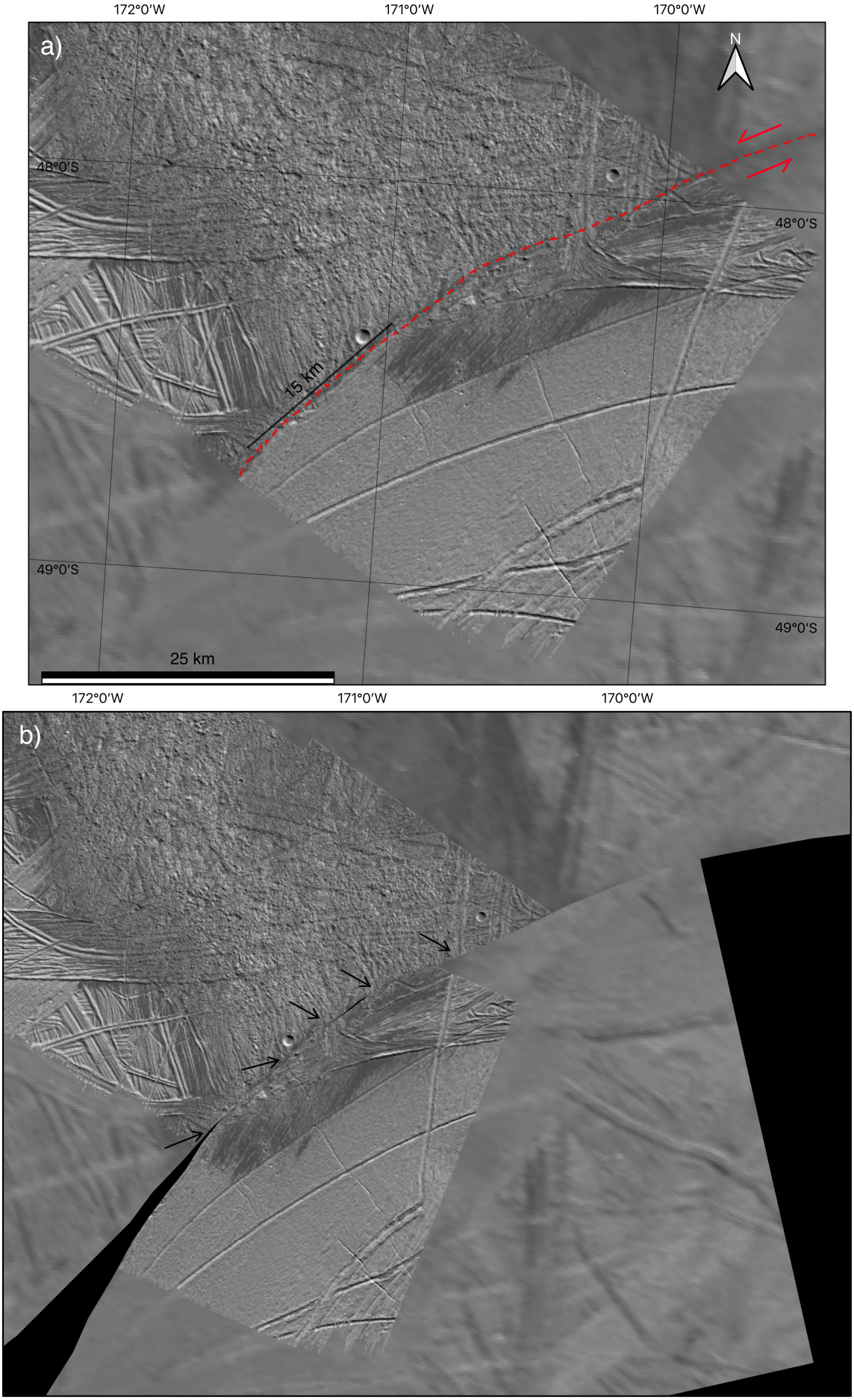
a)
172°0′W
171°0′W
170°0′W
N
48°0′S
48°0′S
15 km
49°0′S
49°0′S
25 km
172°0′W
171°0′W
170°0′W
b)

Figure 6. Location corresponding to Figure 5. (a) Geological setting at the time of data acquisition around the contact between Thrace Macula and Libya Linea. Left-lateral strike-slip fault trace (fault 1 in Figure 5a) shown as a dashed red line, with 15 km displacement (see Figure 5a for a detailed structural interpretation). (b) Reconstruction of geological setting before proposed fault 1 onset (corresponding to the third stage of the sequence of events described in Section 4). Black arrows mark some of the points where the two sides of the fault show the best match.

4 Discussion

Strike-slip tectonic settings are widely common on Earth (Donzé et al., 2021). They have also been observed on terrestrial planets (e.g., Mars, Andrews-Hanna et al., 2008; G. Schmidt et al., 2022) and other ocean worlds, Ganymede (e.g., Rossi et al., 2018), Enceladus (e.g., Rossi et al., 2020), and Titan (e.g., Burkhard et al., 2022; Matteoni et al., 2020). Several other examples also exist on Europa, such as along Agenor Linea in the southern trailing hemisphere and Astypalaea Linea in the south polar region (Hoyer et al., 2014; Kattenhorn, 2004; Prockter et al., 2000; Tufts et al., 1999, 2000). The identification of strike-slip faults on Europa has also led to the recognition that some fractures in the ice shell are not caused primarily by global tidal stresses but are instead resulting from lateral motions along strike-slip faults. These curved secondary tension fractures are termed tailcracks (see Section 3), yet sometimes also indicated as wing cracks, kinks, or horsetail fractures (Kattenhorn, 2004; Kattenhorn & Marshall, 2006; Prockter et al., 2000). Agenor Linea is a ~1500-km-long prominent bright band in Europa's southern hemisphere (Figure 1) that has undergone up to 20 km of right-lateral offset. Its current configuration might have resulted from a varied history of strike-slip and dilational motion (Hoyer et al., 2014; Prockter et al., 2000). At its eastern tip, Agenor exhibits at least six well-developed, trough-like tailcracks that curve towards the south, indicating right-lateral strike-slip motion (Kattenhorn, 2004; Kattenhorn & Marshall, 2006; Prockter et al., 2000). In Figure 3, the numbered (1-4) linear features bordering and intersecting Thrace Macula are the southern continuation of these tailcracks, which demonstrates their strike-slip origin. At locations where these tailcracks intersect Thrace, the latter always crosscuts and disrupts them, proving Thrace's relatively younger age in comparison to the tailcracks and Agenor Linea, from which they originate.

Boundaries of chaos terrains are commonly accompanied by deposits of smooth dark material. Low-albedo material around the edges of Thrace indeed shows evidence of embayment, confinement by topography, and lobate morphologies (Fagents, 2003). Whether this is due to liquid coming from the subsurface (Fagents, 2003) or from the sublimation of bright surface frosts (Fagents et al., 2000) is unclear. Similar dark deposits infilling between ridges are seen around Castalia Macula, a large dark area next to a chaos terrain. A stereo DTM of that area shows that while the dark material is confined to topographic lows, it is far from flat, so a simple explanation of pooling liquids does not fit the observations unless substantial surface motion has taken place afterward and/or material has drained back into the interior (Prockter & Schenk, 2005).

The structural mapping we conducted led to the identification of several strike-slip faults and lineaments, bordering Thrace Macula along most sides (Figure 3). In many cases, these

linear structures continue into it, although their morphologies become distinctly altered, suggesting in situ modification of background terrain by the mechanisms that formed Thrace Macula and therefore proving its relatively young age, as previously noted (Collins & Nimmo, 2009; Kortz et al., 2000; Prockter & Schenk, 2016; B. E. Schmidt et al., 2012). Moreover, in most cases, where lineaments run parallel to Thrace Macula sharp albedo changes are present (Figures 3, 4, and 5). This suggests that preexisting linear structures might act as impermeable barriers for fluids, impeding the further migration of - low albedo - partially molten materials or brines (Aydin, 2006). Therefore, preexisting linear structures likely have constrained Thrace Macula's emplacement and areal distribution, although some may be coeval with the formation of Thrace and could be the result of loading on the surface, such as at Murias Chaos (Figueredo, 2002).

At Thrace Macula's southernmost tip, our interpretation (see Section 3) of a left-lateral strike-slip fault (indicated as 1 in Figure 5a) marking the contact between Thrace Macula and Libya Linea suggests that such tectonic activity, driven by Libya Linea, has displaced a portion of Thrace, as dark material (indicated as 4 in Figure 5a) most likely originating from Thrace (along with other features belonging to Thrace present along the contact) is displaced by ~15 km from the SW towards the NE. A reconstruction of the geological setting before the proposed onset of fault 1 is shown in Figure 6b. This deformation event probably occurred over a relatively long period, as the structures formed are complex and the offset is substantial. The presence of the dark material along fault 1, to the NE of Thrace Macula (white dashed sketch line in Figure 5b), suggests a different behavior for those lineaments whose most recent activity postdate Thrace, in comparison to those that predate it and act as fluid barriers. Indeed, in the early deformation stages, these faults might act as conduits for fluids (Aydin, 2006). Subsurface material originating from Thrace can infiltrate along them and spread on the surface, as it is unconfined (what we likely observe in the area highlighted by the dashed white line in Figure 5b). This material then represents the freshest that could be encountered and sampled by future space missions, such as *Europa Clipper*. Over time, the fault might act as a barrier for the further spreading of fluids, as previously emplaced material freezes and blocks the exchange between the surface and the subsurface (Aydin, 2006).

The presence of the lineament indicated as 5 in Figure 5a, which we interpret as a right-lateral strike-slip fault due to the orientation of tailcracks at its southern tip (Kattenhorn, 2004; Kattenhorn & Marshall, 2006) needs to be explained, to support the interpretation given above in which Thrace Macula is crosscut by a left-lateral strike-slip fault with a ~15 km offset (indicated as fault 1 in Figure 5a), whose activity is driven by Libya Linea. Lineament 5 seems to be present within both Thrace and Libya and to be crosscut and displaced by fault 1 (Figure 6b). Although, within Thrace, lineament 5 is highly disrupted and disaggregated, suggesting its older age in comparison to it (Figure 5). Concurrently, within Libya, it is not disrupted, and it crosscuts every other structure and lineament present, indicating its younger age in comparison to Libya, regardless of our interpretation of lineament 5 as a strike-slip fault due to the presence of tailcracks (Figure 5). It could be then argued that the two portions of lineament 5 are instead two separate lineaments formed at different times. Nevertheless, even if its northernmost observable extent is corresponding to the edge of the high-resolution image 9800r and north of this area only low-resolution images are present, we could not find a continuation for lineament 5 (its portion within Libya) northern of the hypothesized fault 1 (Figure 5).

Considering all the above-mentioned observations and given the perfect match of the two portions of lineament 5 displayed in the reconstruction shown in Figure 6b, along with that of several other portions of the Thrace-Libya contact, we favor an interpretation of lineament 5 as being continuous at the time of fault 1 onset and formed after Libya Linea (and crosscutting the lineaments and structures contained within Libya) yet predating the emplacement of Thrace Macula (which then disrupts it). Left-lateral strike-slip tectonic activity along fault 1, related to the dynamics of Libya Linea, seems to be the most recent event in this area, at least relative to the interaction Thrace-Libya. This interpretation seems the one that best fits all the above-mentioned observations, even if it is partially limited by the quality of the available data.

To summarize, we propose the following sequence of events to explain the observed complex interaction between Thrace Macula and Libya Linea:

1. Formation of the smooth band Libya Linea.
2. Imposition of lineament 5 (likely a right-lateral strike-slip fault, based on the presence and orientation of tailcracks at its southern tip), on both Libya Linea and on the area north of it that will later be occupied by Thrace Macula.
3. Emplacement of the chaos terrain Thrace Macula, in a vast area comprising also the northernmost local portions of Libya Linea (testified by the presence of a dark material patch onto Libya Linea, indicated as 4 in Figure 5a) and disruption of lineament 5 by Thrace Macula (this stage of the sequence corresponds to the setting shown in Figure 6b).
4. Activation (or possible reactivation) of fault 1 as a left-lateral strike-slip fault, driven by Libya Linea's dynamics. Fault 1 has crosscut lineament 5 and parts of Thrace Macula (among other features, the dark material patch marked as 4 in Figure 5a), dislocating by ~15 km all these features.

Our relative age argument for tectonic activity related to Libya Linea postdating the emplacement of Thrace Macula can be further extended, with Agenor Linea now determined to be older than both these two regional-scale structures, as tailcracks originating at its easternmost tip (Kattenhorn, 2004; Prockter et al., 2000) - its most recently formed features - are always being intensely altered in correspondence of Thrace Macula and therefore predate it (Figures 1 and 3). Nonetheless, Agenor is considered to be geologically young (Hoyer et al., 2014), thus, our findings suggest that all these three structures - Agenor, Libya, and Thrace - are relatively young geological features on Europa's surface.

The 26 km dilational displacement with a minor lateral offset, among two portions of a dark double ridge, immediately to the east of the contact between Thrace Macula and Libya Linea (centered at 48.5°S, 169.5°W, yellow dashed line in Figure 5a), whose direction also exactly matches in the tectonic reconstruction shown in Figure 6b, hints either at a multistage tectonic evolution of Libya Linea with different strike-slip and extensional phases in a varying stress field (as it has been proposed for Agenor Linea, Hoyer et al., 2014; Kattenhorn, 2004) or to the fact that transtension (i.e., strike-slip motion with an extensional component, Fossen et al., 1994) has been dominant within Libya Linea at a previous stage of its evolution. An in-depth analysis of the varying tectonic setting along the whole Libya Linea would be necessary to determine which of these two hypotheses should be favored, a goal that goes beyond the scope of

463 the present work. It is, however, worth noting that local transtension has already been observed
464 in other parts of Libya Linea (e.g., Matteoni et al., 2022, preprint).

465

466 **4 Conclusions**

467 In summary, through the present structural mapping study, we are able to determine that:

468 • Several preexisting strike-slip faults and linear structures border Thrace Macula
469 along most sides, the majority of which likely have constrained Thrace's
470 emplacement and areal distribution.

471 • The stratigraphy of the most important features in this portion of Europa's
472 surface is represented by a sequence of events involving the formation of Agenor
473 Linea, followed by that of Libya Linea first and Thrace Macula later, and
474 ultimately by strike-slip tectonic activity driven by Libya Linea and displacing a
475 portion of Thrace Macula by ~15 km.

476 • Thrace Macula is a relatively young feature, as was previously noted, yet some of
477 its parts have been displaced by strike-slip tectonics driven by Libya Linea. Such
478 tectonic activity is the most recent event, within the studied area, that has
479 interested Thrace. The related faults might act as conduits for (uprising) Thrace's
480 subsurface material, which then likely represents the freshest possible that could
481 be sampled by future spacecraft in this region, a major consideration for the
482 upcoming *Europa Clipper* mission and specifically the SUDA instrument.

483 • Our findings are more consistent with a formation model for the chaos terrain
484 Thrace Macula that involves slow diapiric emplacement (e.g., Figueredo, 2002;
485 Mével & Mercier, 2007; Pappalardo et al., 1998; Rathbun et al., 1998; Schenk &
486 Pappalardo, 2004), or brine mobilization driven by diapirism (e.g., Collins et al.,
487 2000; Head & Pappalardo, 1999), rather than with a model involving the quicker
488 and more recent collapse of a melt-lens (e.g., B. E. Schmidt et al., 2011).

489

490

491 **Acknowledgments**

492 We very gratefully thank Louise Prockter, Paul Schenk, and Gianluca Chiarolanza for the
493 insightful discussions, and Björn Schreiner for providing the reconstruction shown in Figure 6b
494 and the related discussions. The research leading to this manuscript received funding from the
495 European Research Council (ERC) under the European Union's Horizon 2020 research and
496 innovation program (ERC Consolidator Grant 724908-Habitat OASIS).

497

498 **Open Research**

499 Data Availability Statement

500

501 *Galileo*'s SSI data used in this manuscript can be accessed from the PDS Cartography and
502 Imaging Science Node (Thaller, 2000), while the SSI photogrammetrically-corrected base map

mosaics can be accessed from the USGS Astrogeology website (Bland & Lynn, 2021). The Digital Terrain Model (Figure 2) and data of the structural map (Figure 3) produced are available on the Freie Universität Berlin Repository - Refubium (Matteoni & Neesemann, 2023).

References

Alexandrov, O., & Beyer, R. A. (2018). Multiview Shape-From-Shading for Planetary Images. *Earth and Space Science*, *5*(10), 652–666. https://doi.org/10.1029/2018EA000390

Andrews-Hanna, J. C., Zuber, M. T., & Hauck, S. A. (2008). Strike-slip faults on Mars: Observations and implications for global tectonics and geodynamics. *Journal of Geophysical Research*, *113*(E8), E08002. https://doi.org/10.1029/2007JE002980

Aydin, A. (2006). Failure modes of the lineaments on Jupiter's moon, Europa: Implications for the evolution of its icy crust. *Journal of Structural Geology*, *28*(12), 2222–2236. https://doi.org/10.1016/j.jsg.2006.08.003

Belton, M. J. S., Klaasen, K. P., Clary, M. C., Anderson, J. L., Anger, C. D., Carr, M. H., et al. (1992). The Galileo Solid-State Imaging experiment. *Space Science Reviews*, *60*(1–4), 413–455. https://doi.org/10.1007/BF00216864

Beyer, R. A., Alexandrov, O., & McMichael, S. (2018). The Ames Stereo Pipeline: NASA's Open Source Software for Deriving and Processing Terrain Data. *Earth and Space Science*, *5*(9), 537–548. https://doi.org/10.1029/2018EA000409

Bierhaus, E. B., & Schenk, P. M. (2010). Constraints on Europa's surface properties from primary and secondary crater morphology. *Journal of Geophysical Research E: Planets*, *115*(12), 1–17. https://doi.org/10.1029/2009JE003451

Bland, M., & Lynn, W. (2021). Photogrammetrically Controlled, Equirectangular Galileo Image Mosaics of Europa [Data set]. U.S. Geological Survey. https://doi.org/10.5066/P9VKKK7C

529 Bland, M. T., Kirk, R. L., Galuszka, D. M., Mayer, D. P., Beyer, R. A., & Fergason, R. L.
530 (2021). How Well Do We Know Europa's Topography? An Evaluation of the Variability in
531 Digital Terrain Models of Europa. *Remote Sensing*, *13*(24), 5097.
532 https://doi.org/10.3390/rs13245097
533 Bland, M. T., Weller, L. A., Archinal, B. A., Smith, E., & Wheeler, B. H. (2021). Improving the
534 Usability of Galileo and Voyager Images of Jupiter's Moon Europa. *Earth and Space*
535 *Science*, *8*(12). https://doi.org/10.1029/2021EA001935
536 Burkhard, L. M. L., Smith-Konter, B. R., Fagents, S. A., Cameron, M. E., Collins, G. C., &
537 Pappalardo, R. T. (2022). Strike-slip faulting on Titan: Modeling tidal stresses and shear
538 failure conditions due to pore fluid interactions. *Icarus*, *371*(March 2021), 114700.
539 https://doi.org/10.1016/j.icarus.2021.114700
540 Carlson, R. W., Johnson, R. E., & Anderson, M. S. (1999). Sulfuric acid on Europa and the
541 radiolytic sulfur cycle. *Science*, *286*(5437), 97–99.
542 https://doi.org/10.1126/science.286.5437.97
543 Carr, M. H., Belton, M. J. S., Chapman, C. R., Davies, M. E., Geissler, P., Greenberg, R., et al.
544 (1998). Evidence for a subsurface ocean on Europa. *Nature*, *391*(6665), 363–365.
545 https://doi.org/10.1038/34857
546 Collins, G., & Nimmo, F. (2009). Chaotic Terrain on Europa. In *Europa* (pp. 259–282).
547 University of Arizona Press. https://doi.org/10.2307/j.ctt1xp3wdw.17
548 Collins, G. C., Head, J. W., Pappalardo, R. T., & Spaun, N. A. (2000). Evaluation of models for
549 the formation of chaotic terrain on Europa. *Journal of Geophysical Research: Planets*,
550 *105*(E1), 1709–1716. https://doi.org/10.1029/1999JE001143
551 Crameri, F. (2021). Scientific colour maps. https://doi.org/10.5281/ZENODO.5501399

552 Crameri, F., Shephard, G. E., & Heron, P. J. (2020). The misuse of colour in science
553 communication. *Nature Communications*, *11*(1), 5444. https://doi.org/10.1038/s41467-020-
554 19160-7
555 Dalton, J. B., Prieto-Ballesteros, O., Kargel, J. S., Jamieson, C. S., Jolivet, J., & Quinn, R.
556 (2005). Spectral comparison of heavily hydrated salts with disrupted terrains on Europa.
557 *Icarus*, *177*(2), 472–490. https://doi.org/10.1016/j.icarus.2005.02.023
558 Doggett, T., Greeley, R., Figueredo, P., & Tanaka, K. (2009). Geologic Stratigraphy and
559 Evolution of Europa's Surface. In *Europa* (pp. 137–160). University of Arizona Press.
560 https://doi.org/10.2307/j.ctt1xp3wdw.12
561 Donzé, F.-V., Klinger, Y., Bonilla-Sierra, V., Duriez, J., Jiao, L., & Scholtès, L. (2021).
562 Assessing the brittle crust thickness from strike-slip fault segments on Earth, Mars and Icy
563 moons. *Tectonophysics*, *805*(May 2020), 228779.
564 https://doi.org/10.1016/j.tecto.2021.228779
565 Fagents, S. A. (2003). Considerations for effusive cryovolcanism on Europa: The post-Galileo
566 perspective. *Journal of Geophysical Research: Planets*, *108*(E12), 13–1.
567 https://doi.org/10.1029/2003JE002128
568 Fagents, S. A., Greeley, R., Sullivan, R. J., Pappalardo, R. T., & Prockter, L. M. (2000).
569 Cryomagmatic Mechanisms for the Formation of Rhadamanthys Linea, Triple Band
570 Margins, and Other Low-Albedo Features on Europa. *Icarus*, *144*(1), 54–88.
571 https://doi.org/10.1006/icar.1999.6254
572 Fagents, S. A., Lopes, R. M. C., Quick, L. C., & Gregg, T. K. P. (2022). Cryovolcanism. In
573 *Planetary Volcanism across the Solar System* (pp. 161–234). Elsevier.
574 https://doi.org/10.1016/B978-0-12-813987-5.00005-5

575 Figueredo, P. H. (2002). Geology and origin of Europa's "Mitten" feature (Murias Chaos).
576 *Journal of Geophysical Research*, *107*(E5), 5026. https://doi.org/10.1029/2001JE001591
577 Figueredo, Patricio H., & Greeley, R. (2004). Resurfacing history of Europa from pole-to-pole
578 geological mapping. *Icarus*, *167*(2), 287–312. https://doi.org/10.1016/j.icarus.2003.09.016
579 Fossen, H., Tikoff, B., & Teyssier, C. (1994). Strain modeling of transpressional and
580 transtensional deformation. *Norsk Geologisk Tidsskrift*, *74*(3), 134–145.
581 Goode, W., Kempf, S., & Schmidt, J. (2021). Detecting the surface composition of geological
582 features on Europa and Ganymede using a surface dust analyzer. *Planetary and Space*
583 *Science*, *208*(September), 105343. https://doi.org/10.1016/j.pss.2021.105343
584 Goode, W., Kempf, S., & Schmidt, J. (2023). Mapping the surface composition of Europa with
585 SUDA. *Planetary and Space Science*, *227*(August 2022), 105633.
586 https://doi.org/10.1016/j.pss.2023.105633
587 Greenberg, R., Hoppa, G. V., Tufts, B. R., Geissler, P., Riley, J., & Kadel, S. (1999). Chaos on
588 Europa. *Icarus*, *141*(2), 263–286. https://doi.org/10.1006/icar.1999.6187
589 Gürbüz, A. (2010). Geometric characteristics of pull-apart basins. *Lithosphere*, *2*(3), 199–206.
590 https://doi.org/10.1130/L36.1
591 Hand, K. P., Carlson, R. W., & Chyba, C. F. (2007). Energy, chemical disequilibrium, and
592 geological constraints on Europa. *Astrobiology*, *7*(6), 1006–1022.
593 https://doi.org/10.1089/ast.2007.0156
594 Hand, K. P., Chyba, C. F., Priscu, J. C., Carlson, R. W., & Nealson, K. H. (2009). Astrobiology
595 and the Potential for Life on Europa. In *Europa* (pp. 589–630).
596 https://doi.org/10.2307/j.ctt1xp3wdw.32
597 Head, J. W., & Pappalardo, R. T. (1999). Brine mobilization during lithospheric heating on

598 Europa: Implications for formation of chaos terrain, lenticula texture, and color variations.
599 *Journal of Geophysical Research E: Planets*, *104*(E11), 27143–27155.
600 https://doi.org/10.1029/1999JE001062
601 Howell, S. M., & Pappalardo, R. T. (2018). Band Formation and Ocean-Surface Interaction on
602 Europa and Ganymede. *Geophysical Research Letters*, *45*(10), 4701–4709.
603 https://doi.org/10.1029/2018GL077594
604 Hoyer, L., Kattenhorn, S. A., & Watkeys, M. K. (2014). Multistage evolution and variable
605 motion history of Agenor Linea, Europa. *Icarus*, *232*, 60–80.
606 https://doi.org/10.1016/j.icarus.2013.12.010
607 Johnson, B. C., Sheppard, R. Y., Pascuzzo, A. C., Fisher, E. A., & Wiggins, S. E. (2017).
608 Porosity and Salt Content Determine if Subduction Can Occur in Europa's Ice Shell.
609 *Journal of Geophysical Research: Planets*, *122*(12), 2765–2778.
610 https://doi.org/10.1002/2017JE005370
611 Kattenhorn, S. A. (2004). Strike-slip fault evolution on Europa: evidence from tailcrack
612 geometries. *Icarus*, *172*(2), 582–602. https://doi.org/10.1016/j.icarus.2004.07.005
613 Kattenhorn, S. A., & Marshall, S. T. (2006). Fault-induced perturbed stress fields and associated
614 tensile and compressive deformation at fault tips in the ice shell of Europa: implications for
615 fault mechanics. *Journal of Structural Geology*, *28*(12), 2204–2221.
616 https://doi.org/10.1016/j.jsg.2005.11.010
617 Kattenhorn, S. A., & Prockter, L. M. (2014). Evidence for subduction in the ice shell of Europa.
618 *Nature Geoscience*, *7*(10), 762–767. https://doi.org/10.1038/ngeo2245
619 Kempf, S., Altobelli, N., Briois, C., Grün, E., Horanyi, M., Postberg, F., et al. (2014). SUDA: A
620 Dust Mass Spectrometer for Compositional Surface Mapping for a Mission to Europa.

European Planetary Science Congress 2014, *9*(EPSC2014-229). Retrieved from http://adsabs.harvard.edu/abs/2014EPSC....9..229K

Kortz, B. E., Head, J. W., & Pappalardo, R. T. (2000). Thrace Macula, Europa: Characteristics of the southern margin and relations to backgrounds plains and Libya Linea (p. 2052).

V. Krivov, A., Sremčević, M., Spahn, F., Dikarev, V. V., & Kholshevnikov, K. V. (2003). Impact-generated dust clouds around planetary satellites: spherically symmetric case. *Planetary and Space Science*, *51*(3), 251–269. https://doi.org/10.1016/S0032-0633(02)00147-2

Lam, T., Buffington, B., & Campagnola, S. (2018). A Robust Mission Tour for NASA's Planned Europa Clipper Mission. In *2018 Space Flight Mechanics Meeting*. Reston, Virginia: American Institute of Aeronautics and Astronautics. https://doi.org/10.2514/6.2018-0202

Leonard, E. J., Pappalardo, R. T., & Yin, A. (2018). Analysis of very-high-resolution Galileo images and implications for resurfacing mechanisms on Europa. *Icarus*, *312*, 100–120. https://doi.org/10.1016/j.icarus.2018.04.016

Lesage, E., Schmidt, F., Andrieu, F., & Massol, H. (2021). Constraints on effusive cryovolcanic eruptions on Europa using topography obtained from Galileo images. *Icarus*, *361*, 114373. https://doi.org/10.1016/j.icarus.2021.114373

Matteoni, P., & Neesemann, A. (2023). Replication data for: Strike-slip tectonic control on the emplacement of Thrace Macula on Europa. https://doi.org/10.17169/refubium-38694

Matteoni, P., Mitri, G., Poggiali, V., & Mastrogiuseppe, M. (2020). Geomorphological Analysis of the Southwestern Margin of Xanadu, Titan: Insights on Tectonics. *Journal of Geophysical Research: Planets*, *125*(12), 1–22. https://doi.org/10.1029/2020JE006407

Matteoni, P., Neesemann, A., Jaumann, R., Hillier, J. K., & Postberg, F. (2022). Ménec Fossae

644 on Europa: a Strike-Slip Tectonics Origin above a possible Shallow Water Reservoir.
645 *Essoar Open Archive*. https://doi.org/10.1002/essoar.10512629.1
646 Mével, L., & Mercier, E. (2007). Large-scale doming on Europa: A model of formation of Thera
647 Macula. *Planetary and Space Science*, *55*(7–8), 915–927.
648 https://doi.org/10.1016/j.pss.2006.12.001
649 Miyamoto, H., Mitri, G., Showman, A. P., & Dohm, J. M. (2005). Putative ice flows on Europa:
650 Geometric patterns and relation to topography collectively constrain material properties and
651 effusion rates. *Icarus*, *177*(2), 413–424. https://doi.org/10.1016/j.icarus.2005.03.014
652 O'Brien, D. (2002). A Melt-through Model for Chaos Formation on Europa. *Icarus*, *156*(1),
653 152–161. https://doi.org/10.1006/icar.2001.6777
654 Pappalardo, R. T., Head, J. W., Greeley, R., Sullivan, R. J., Pilcher, C., Schubert, G., et al.
655 (1998). Geological evidence for solid-state convection in Europa's ice shell. *Nature*,
656 *391*(6665), 365–368. https://doi.org/10.1038/34862
657 Postberg, F., Grün, E., Horanyi, M., Kempf, S., Krüger, H., Schmidt, J., et al. (2011).
658 Compositional mapping of planetary moons by mass spectrometry of dust ejecta. *Planetary*
659 *and Space Science*, *59*(14), 1815–1825. https://doi.org/10.1016/j.pss.2011.05.001
660 Prockter, L., & Schenk, P. (2005). Origin and evolution of Castalia Macula, an anomalous young
661 depression on Europa. *Icarus*, *177*(2), 305–326. https://doi.org/10.1016/j.icarus.2005.08.003
662 Prockter, L. M., & Schenk, P. M. (2016). The geological context and history of Thrace Macula,
663 Europa. In *47th Annual Lunar and Planetary Science Conference* (p. 1673).
664 Prockter, L. M., Pappalardo, R. T., & Head, J. W. (2000). Strike-slip duplexing on Jupiter's icy
665 moon Europa. *Journal of Geophysical Research: Planets*, *105*(E4), 9483–9488.
666 https://doi.org/10.1029/1999JE001226

667 Quick, L. C., Glaze, L. S., & Baloga, S. M. (2017). Cryovolcanic emplacement of domes on
668 Europa. *Icarus*, *284*, 477–488. https://doi.org/10.1016/j.icarus.2016.06.029
669 Rathbun, J. A., Musser, G. S., & Squyres, S. W. (1998). Ice diapirs on Europa: Implications for
670 liquid water. *Geophysical Research Letters*, *25*(22), 4157–4160.
671 https://doi.org/10.1029/1998GL900135
672 Rossi, C., Cianfarra, P., Salvini, F., Mitri, G., & Massé, M. (2018). Evidence of transpressional
673 tectonics on the Uruk Sulcus region, Ganymede. *Tectonophysics*, *749*(March), 72–87.
674 https://doi.org/10.1016/j.tecto.2018.10.026
675 Rossi, C., Cianfarra, P., Salvini, F., Bourgeois, O., & Tobie, G. (2020). Tectonics of Enceladus'
676 South Pole: Block Rotation of the Tiger Stripes. *Journal of Geophysical Research: Planets*,
677 *125*(12), 1–21. https://doi.org/10.1029/2020JE006471
678 Schenk, P., Matsuyama, I., & Nimmo, F. (2020). A Very Young Age for True Polar Wander on
679 Europa From Related Fracturing. *Geophysical Research Letters*, *47*(17), 1–9.
680 https://doi.org/10.1029/2020GL088364
681 Schenk, P. M., & Pappalardo, R. T. (2004). Topographic variations in chaos on Europa:
682 Implications for diapiric formation. *Geophysical Research Letters*, *31*(16), 1–5.
683 https://doi.org/10.1029/2004GL019978
684 Schmidt, B. E., Blankenship, D. D., Patterson, G. W., & Schenk, P. M. (2011). Active formation
685 of 'chaos terrain' over shallow subsurface water on Europa. *Nature*, *479*(7374), 502–505.
686 https://doi.org/10.1038/nature10608
687 Schmidt, B. E., Blankenship, D. D., Patterson, G. W., & Schenk, P. M. (2012). Insights into
688 Europa's shallow water mobility from Thrace and Thera Macula. In *43rd Annual Lunar and*
689 *Planetary Science Conference* (Vol. 1659, p. 2267).

690 Schmidt, G., Luzzi, E., Rossi, A. P., Pondrelli, M., Apuzzo, A., & Salvini, F. (2022). Protracted
691 Hydrogeological Activity in Arabia Terra, Mars: Evidence from the Structure and
692 Mineralogy of the Layered Deposits of Becquerel Crater. *Journal of Geophysical Research:*
693 *Planets*. https://doi.org/10.1029/2022JE007320
694 Soderlund, K. M., Schmidt, B. E., Wicht, J., & Blankenship, D. D. (2014). Ocean-driven heating
695 of Europa's icy shell at low latitudes. *Nature Geoscience*, *7*(1), 16–19.
696 https://doi.org/10.1038/ngeo2021
697 Spaun, N. A., Head, J. W., Collins, G. C., Prockter, L. M., & Pappalardo, R. T. (1999).
698 Conamara Chaos Region, Europa: Reconstruction of mobile polygonal ice blocks.
699 *Geophysical Research Letters*, *25*(23), 4277–4280. https://doi.org/10.1029/1998GL900176
700 Thomas F. Thaller. (2000). GALILEO ORBITAL OPERATIONS SOLID STATE IMAGING
701 RAW EDR V1.0 [Data set]. NASA Planetary Data System.
702 https://doi.org/10.17189/1520425
703 Trumbo, S. K., Brown, M. E., & Hand, K. P. (2019a). H 2 O 2 within Chaos Terrain on Europa's
704 Leading Hemisphere. *The Astronomical Journal*, *158*(3), 127. https://doi.org/10.3847/1538-
705 3881/ab380c
706 Trumbo, S. K., Brown, M. E., & Hand, K. P. (2019b). Sodium chloride on the surface of Europa.
707 *Science Advances*, *5*(6), 2–6. https://doi.org/10.1126/sciadv.aaw7123
708 Trumbo, S. K., Becker, T. M., Brown, M. E., Denman, W. T. P., Molyneux, P., Hendrix, A., et
709 al. (2022). A New UV Spectral Feature on Europa: Confirmation of NaCl in Leading-
710 hemisphere Chaos Terrain. *The Planetary Science Journal*, *3*(2), 27.
711 https://doi.org/10.3847/PSJ/ac4580
712 Tufts, B. R., Greenberg, R., Hoppa, G., & Geissler, P. (1999). Astypalaea Linea: A Large-Scale

713 Strike-Slip Fault on Europa. *Icarus*, *141*(1), 53–64. https://doi.org/10.1006/icar.1999.6168
714 Tufts, B. R., Greenberg, R., Hoppa, G., & Geissler, P. (2000). Lithospheric Dilation on Europa.
715 *Icarus*, *146*(1), 75–97. https://doi.org/10.1006/icar.2000.6369
716 Vance, S. D., Hand, K. P., & Pappalardo, R. T. (2016). Geophysical controls of chemical
717 disequilibria in Europa. *Geophysical Research Letters*, *43*(10), 4871–4879.
718 https://doi.org/10.1002/2016GL068547
719 Wilson, L., Head, J. W., & Pappalardo, R. T. (1997). Eruption of lava flows on Europa: Theory
720 and application to Thrace Macula. *Journal of Geophysical Research: Planets*, *102*(E4),
721 9263–9272. https://doi.org/10.1029/97JE00412
722